Journal of
Materials Chemistry B

PAPER

View Article Online
View Journal | View Issue

Cite this: *J. Mater. Chem. B*, 2024, **12**, 5848

Peptide nanovaccine conjugated *via* a retro-Diels–Alder reaction linker for overcoming the obstacle in lymph node penetration and eliciting robust cellular immunity†

Kuncheng Lv,[ab] Sheng Ma,[ac] Liping Liu,[ab] Hongyu Chen,[ab] Zichao Huang,[ab]
Zhenyi Zhu,[ab] Yibo Qi[ab] and Wantong Song *[abc]

Received 30th March 2024,
Accepted 6th May 2024

DOI: 10.1039/d4tb00674g

rsc.li/materials-b

Nanoparticles have been regarded as a promising vaccine adjuvant due to their innate immune potentiation and enhanced antigen transport. However, the inefficient infiltration into the lymph node (LN) paracortex of nanoparticles caused by subcapsular sinus (SCS) obstruction is the main challenge in further improvement of nanovaccine immune efficacy. Herein, we propose to overcome paracortex penetration by using nanovaccine to spontaneously and continuously release antigens after retention in the SCS. In detail, we utilized a spontaneous retro-Diels–Alder (r-D–A) reaction linker to connect poly{(2-methyl-2-oxazoline)$_{80}$-*co*-[(2-butyl-2-oxazoline)$_{15}$-*r*-(2-thioethyl-2-oxazoline)$_8$]} (PMBOxSH) and peptides for the peptide nanovaccine construction. The r-D–A reaction linker can spontaneously break over time, allowing the nanovaccine to release free antigens and adjuvants upon reaching the LN, thereby facilitating the entry of released antigens and adjuvants into the interior of the LNs. We showed that the efficacy of the peptide nanovaccine constructed using this dynamic linker could be significantly improved, thus greatly enhancing the tumor inhibition efficacy in the B16-OVA model. This dynamic-covalent-chemistry-based vaccine strategy may inspire designing more efficient therapeutic vaccines, especially those that require eliciting high-amount T cell responses.

Introduction

Cancer vaccines offer a promising strategy for combating malignancies.[1] Among these, peptide-based cancer vaccines have gained significant attention due to their rapid preparation[2,3] and clinical application.[4–6] However, challenges such as antigen instability have prompted the adoption of nano-encapsulation technology to enhance vaccine efficacy.[7] Nanoparticles possess inherent properties that facilitate their accumulation in LNs and uptake by antigen presenting cells (APCs),[8–12] thereby enhancing vaccine efficacy. Nevertheless, recent investigations have revealed that a considerable proportion of nanoparticles reaching LNs are trapped in the subcapsular sinus (SCS) rather than penetrating into the LNs.[13,14] Notably, particle size emerges as a critical determinant, with larger nanoparticles exhibiting a higher propensity for entrapment compared to their smaller counterparts capable of traversing the SCS.[14–16] Given that dendritic cells (DCs)

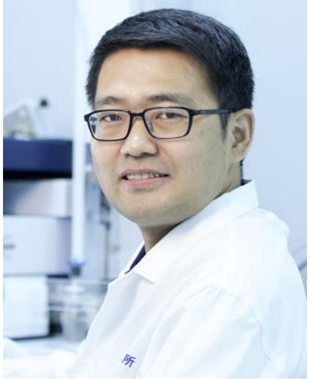

Wantong Song

Dr. Wantong Song is a Professor at the Changchun Institute of Applied Chemistry, Chinese Academy of Sciences. He received his BSc degree in applied chemistry from Nanjing University and PhD degree in polymer chemistry from the University of Chinese Academy of Sciences. He was a National Institute of Health (NIH) T32 Associated postdoctoral fellow at the University of North Carolina at Chapel Hill. Dr Song's lab now focuses on developing the next generation delivery vehicles for mRNA and vaccines through a unique combination of polymer chemistry, high throughput screening and artificial intelligence. He is the recipient of the U.S. Chinese Anti-Cancer Association (USCACA) Scholar Award, and Chinese-American Society of Nanomedicine and Nanotechnology (CASNN) Rising Star Award.

---

[a] *Key Laboratory of Polymer Ecomaterials, Changchun Institute of Applied Chemistry, Chinese Academy of Sciences, Changchun 130022, China. E-mail: wtsong@ciac.ac.cn*

[b] *School of Applied Chemistry and Engineering, University of Science and Technology of China, Hefei 230026, China*

[c] *Jilin Biomedical Polymers Engineering Laboratory, Changchun 130022, China*

† Electronic supplementary information (ESI) available. See DOI: https://doi.org/10.1039/d4tb00674g

and T cells within the deep paracortex zone primarily orchestrate cellular immunity,[17,18] the restricted accessibility of nanoparticles to these regions represents a significant barrier hindering the elicitation of robust T cell-mediated immune responses.

Nanoparticles engineered for intelligent transformation have been widely used in drug delivery.[19–21] In tumor tissues, the design of drug carriers sensitive to pH, reactive oxygen species (ROS), glutathione (GSH),[22–26] *etc.*, and the transformation of particle size,[27–29] surface potential,[30–32] and other characteristics[33–36] upon arrival in tumor tissues can increase the penetration into the tumor. However, for LNs, there is no stimulus response signal, which poses a challenge for the design of intelligent transformation materials.[37]

Dynamic covalent bonds (DCBs) are a class of bonds which can be transformed spontaneously under certain conditions over time.[38,39] Such bonds include imine bonds,[40] acylhydrazone bonds,[41] double bonds from the Diels–Alder (D–A) reaction,[42] *etc.*, and have been used in the design of self-repairing materials. Among them, the imine bond and acylhydrazone bond can undergo reversible conversions under different pH conditions, while the r-D–A reaction is independent of the solution pH but typically requires elevated temperatures (>100 °C) for effective execution.[43] It is noteworthy that Casida *et al.* found that furans and disubstituted alkynes undergo the D–A reaction to yield bicyclic dienes with thiol reactivity, and the resulting products can spontaneously undergo cleavage under physiological conditions *via* the r-D–A reaction.[44] Further control over the rate of the r-D–A reaction has been achieved by Finn *et al.* through the introduction of functional groups such as methyl, trifluoromethyl, and dimethyl ester onto the bicyclic dienes.[45,46] Therefore, the bicyclic dienes, referred to as oxanorbornadiene (OND), can be used as a linker to control the release rate without external stimulus signals, thus meeting the requirements of transport to and release in LNs.

In this study, we proposed an idea to control the release of antigens and adjuvants by using the r-D–A reaction of OND-thiol adducts to address the problem of no stimulus signal and the need for intelligent transformation to promote penetration in LNs. Specifically, the antigens and adjuvants were conjugated to the PMBOxSH carrier *via* an OND linker and assembled into nanoparticles. Upon reaching the cortex area of the LNs, the r-D–A reaction occurred, leading to the gradual release of antigens and adjuvants. Consequently, these released components diffused deeper into the regions of DCs and T cells within the LNs, thereby activating CD8$^+$ antigen-specific T cell immunity. We showed that r-D–A linker based nanovaccines could elicit much more efficient cellular immune responses and resulted in a more efficacious tumor inhibition effect as tumor vaccines.

Material and methods/experiment

Materials

Valeric acid, *n*-butyl mercaptan, 3-maleimidopropionic acid and iso-butyl chloroformate were purchased from Shanghai Macklin Biochemical Technology Co., Ltd (Shanghai, China). Glutaric anhydride was purchased from Shanghai Bide Pharmaceutical Technology Co., Ltd (Shanghai, China). 2-Methyl-2-oxazoline, triethylamine (TEA), 3-mercaptopropionic acid (3-MPA), methyl trifluoromethylsulfonate (MeOTf), 2-chloroethanamine hydrochloride, furfurylamine, piperazine, fluorescein 5-isothiocyanate (FITC), tetrahydrofuran (THF, dry), dimethylformamide (DMF, dry), ethyl acetate (EA), hexane (HEX), dimethyl sulfoxide (DMSO), dichloromethane (DCM) and dimethyl acetylenedicarboxylate were purchased from Energy Chemical Co., Ltd (Shanghai, China). *N*,*N*-Diisopropylethylamine (DIPEA), trimethylaluminum and rhodamine B (RhoB) were purchased from Shanghai Aladdin Biochemical Technology Co., Ltd (Shanghai, China). 4-Methoxybenzyl chloride, 1-(3-dimethylaminopropyl)-3-ethylcarbodiimide (hydrochloride) (EDCI) and *N*-hydroxysuccinimide (NHS) were purchased from Shanghai Haohong Biomedical Technology Co., Ltd (Shanghai, China). OVA peptide$_{257–264}$ (SIINFEKL) was purchased from Shanghai Sangon Biotech Co., Ltd. IMDQ (CAS: 1258457-59-8) was purchased from Suzhou Nuobeike Biotechnology Co. Ltd. All other reagents and solvents were obtained from Sinopharm Group Co., Ltd.

Characterization

^{1}H NMR spectra were acquired using a Bruker AV-300 or AV-500 NMR spectrometers, utilizing either $CDCl_3$ or CD_3OD as solvents. ^{13}C NMR spectra were obtained on a Bruker AV-300 NMR spectrometer, with $CDCl_3$ employed as the solvent. UV-HPLC analysis was conducted on an Eclassical 3100 system of Elite Analytical Instrument, equipped with an Elite C18 column (5 μm, 4.6 mm × 250 mm). Molecular weight parameters, including the number-averaged molecular weight (M_n) and polydispersity index (PDI), were determined using gel permeation chromatography (GPC) employing a Waters 1515 pump and 2414 detector. Flow cytometry experiments were performed using a BD flow cytometer (BD FACSCelesta™, USA). Particle sizes were measured on a Malvern Zetasizer instrument by the dynamic light scattering method (Nano-ZS90, England). Samples were imaged using a transmission electron microscope (TEM), specifically the FEI Tecnai G2 S-Twin equipped with a field emission gun operating at 200 kV. Scanning fluorescence spectra were recorded using the F-320 fluorescence spectrophotometer from TIANJIN GANGDONG SCI.&TECH. CO., Ltd. All immunofluorescence slides were imaged using a confocal laser scanning microscope (CLSM), specifically the Carl Zeiss LSM 700 model from Germany. *Ex vivo* fluorescence images of LNs were captured using IVIS Lumina LT III (PE, USA).

Cell lines

B16-OVA cells (murine B16 melanoma cells expressing OVA protein) were cultured in RPMI-1640 (containing 10% FBS, 100 U mL^{-1} penicillin, and 100 μg mL^{-1} streptomycin) at 37 °C undrer an atmosphere of 5% CO_2.

Bone marrow-derived dendritic cells (BMDCs) were extracted from the bone marrow of C57BL/6 mice. Mice aged 4 to 6 weeks were euthanized, and femurs and tibias were removed to isolate bone marrow cells. These cells were then transferred to RPMI-1640 complete culture medium supplemented with GM-CSF and IL-4 at concentrations of 20 ng mL^{-1} and 10 ng mL^{-1}, respectively. The medium was changed every two days using a half-media exchange method, and BMDCs were collected on the 7th day.

Animal declaration

All animal experiments adhered to the guidelines sanctioned by the Animal Welfare and Ethics Committee of Changchun Institute of Applied Chemistry, Chinese Academy of Sciences (2022-0026). Female C57BL/6 mice aged 6–8 weeks were procured from Beijing Vital River Laboratory Animal Technology Co. Ltd (Beijing, China). Upon reaching a tumor volume of 2000 mm^3, the mice were euthanized and documented as deceased.

Characterization of free thiol groups

A solution of 3.9 mg FITC (10.0 μmol) was prepared in 10 mL of anhydrous DMSO. Subsequently, a 0.1 mL aliquot of this solution was withdrawn and diluted to 3 mL using Na_2CO_3/$NaHCO_3$ buffer (pH = 10). Nine centrifuge tubes were prepared, each receiving 0.1 mL of the diluted FITC solution. Among these, three tubes were diluted to 1 mL with buffer to serve as blank controls, three tubes received 1.0 mg of 3-MPA (9.3 μmol), and were then diluted to 1 mL with buffer, and the final three tubes received 11.4 mg of PMBOxSH, followed by dilution to 1 mL with buffer. After a 5-minute incubation, scanning fluorescence spectra of the samples between 500 and 650 nm were recorded using an excitation wavelength of 494 nm.

Characterization of the reaction process between OND and *n*-butyl mercaptan

To determine the reaction time for the formation of adducts between OND and thiol groups, 8.4 mg of *n*-butyl mercaptan (93.3 μmol) and 22.0 mg of OND (62.3 μmol) were dissolved in CD_3OD, followed by the addition of 8.7 mg of TEA (86.0 μmol). After vortexing, the mixed solution was transferred to an NMR tube and subsequently positioned within a shaker at a temperature of 37 °C for incubation. ^{1}H-NMR spectra were recorded at 30 minutes and 60 minutes to monitor the reaction progress by comparing the spectra.

After determining the reaction conditions between the OND and the thiol group, we further investigated the rate of adduct formation between OND and *n*-butyl mercaptan, as well as the effect of temperature on the rate of adduct dissociation. Specifically, 42.0 mg of *n*-butyl mercaptan (466.5 μmol) and 110.0 mg of OND (311.5 μmol) were dissolved in CD_3OD, followed by the addition of 43.5 mg of TEA (430.0 μmol). The mixed solution was vortexed and then incubated in a shaker at 37 °C for 1 hour. Subsequently, the mixture was divided into equal portions and transferred into five NMR tubes, which were then stored under different temperature conditions: 37 °C, 20 °C, 4 °C, −24 °C, and −80 °C. Immediately after preparation, ^{1}H-NMR spectra were recorded, marking the start as 0 hours. Subsequently, ^{1}H-NMR spectra were recorded at 12 hours, 24 hours, 48 hours, 84 hours, 120 hours, 192 hours, and 288 hours to monitor the progression of the reaction over time. The rate of adduct dissociation was determined by comparing spectra and monitoring changes in the integration values of peaks near a chemical shift of 7.4 ppm.

Preparation of nanovaccines

70 mg of PMBOxSH was dissolved in 5 mL of methanol, followed by the addition of 30.7 mg of OND (86.9 μmol) and 13.2 mg of TEA (130.0 μmol). The reaction was carried out at 37 °C for 1 hour. After the reaction, dialysis against methanol at 0 °C was conducted for 24 hours. Subsequently, the solvent was eliminated through rotary evaporation, and the residue was dissolved in 5 mL of DMF. To this solution, 12.5 mg of EDCI (65.2 μmol) and 7.5 mg of NHS (65.2 μmol) were added, followed by stirring at room temperature for 30 minutes. Then, 13.48 mg of OVA $peptide_{257-264}$ (14.0 μmol) and 5.03 mg of IMDQ (14.0 μmol) were added to the mixture, which was then subjected to a reaction at 0 °C for a duration of 12 hours with HPLC monitoring. After the reaction, dialysis against DMF at 0 °C was conducted gradually exchanging DMF to PBS. After 24 hours, the liquid from the dialysis bag was transferred to a beaker and supplemented with PBS, yielding the PMBOxS-OND-OVA/IMDQ nanovaccine.

Following the same procedure, replacing OND with 3-maleimidopropionic acid yields PMBOxS-Mal-OVA/IMDQ. Similarly, replacing OVA $peptide_{257-264}$ and IMDQ with RhoB piperazine amide yields PMBOxS-OND-Rhodamine and PMBOxS-Mal-Rhodamine, respectively.

Characterization of *in vitro* release of nanovaccines

RhoB piperazine amide, PMBOxS-Mal-Rhodamine, and PMBOxS-OND-Rhodamine were dissolved separately in PBS. The absorbance intensity of each solution was measured using a UV-visible spectrophotometer, and they were diluted to ensure consistent absorbance intensity. Subsequently, 5 mL of each diluted solution was transferred into three dialysis bags, which were then placed in three separate beakers containing 100 mL of PBS each. The beakers were incubated in a shaker at 37 °C. Periodically, 0.5 mL of solution was withdrawn from each beaker and replaced with 0.5 mL of fresh PBS. The absorbance spectra of the withdrawn solutions were measured using a UV-visible spectrophotometer. The release amount at each time point was determined based on a standard curve.

BMDC activation and antigen cross-presentation *in vitro*

For the *in vitro* DC activation assay, BMDCs were seeded in a 24-well plate at a density of 3.5 × 10^5 cells per well. Nanovaccines containing 5 μg mL^{-1} OVA $peptide_{257-264}$ were introduced to each well. Following a 6-hour incubation period, the cells were harvested and processed. Subsequent staining with antibodies (FITC anti-mouse CD11c antibody, APC-Cy7 anti-mouse MHC II (major histocompatibility complex class II) antibody and PE/Cy7 anti-mouse CD86 antibody) was performed, followed by analysis *via* flow cytometry.

Similarly, in the *in vitro* antigen cross-presentation assay, BMDCs were plated in a 24-well plate at a density of 3.5 × 10^5 cells per well. Nanovaccines containing 5 μg mL^{-1} OVA peptide$_{257-264}$ were introduced into each well. Following a 24-hour incubation period, the cells were collected and processed. They were stained with antibodies (FITC anti-mouse CD11c antibody and PE anti-mouse H2Kb/SIINFEKL antibody) and analyzed using flow cytometry.

DC activation and antigen cross-presentation *in vivo*

In the *in vivo* DC activation experiment, female C57BL/6 mice were administered a subcutaneous injection of 100 μL of nanovaccine, which contained 20 μg of OVA peptide$_{257-264}$. After 48 hours, mice were euthanized, and inguinal LNs were harvested and processed by grinding and filtering through a 300-mesh nylon strainer. The collected single-cell suspension was stained with antibodies (FITC anti-mouse CD11c antibody, APC anti-mouse CD80 antibody and PE/Cy7 anti-mouse CD86 antibody) and analyzed using flow cytometry.

For the *in vivo* antigen cross-presentation experiment, female C57BL/6 mice were subcutaneously injected with 100 μL of nanovaccine containing 20 μg of OVA peptide$_{257-264}$. After 48 hours, mice were euthanized, and inguinal LNs were harvested and processed by grinding and filtering through a 300-mesh nylon strainer. The collected single-cell suspension was stained with antibodies (FITC anti-mouse CD11c antibody and PE anti-mouse H2Kb/SIINFEKL antibody) and analyzed using flow cytometry.

Lymph node accumulation analysis

RhoB, PMBOxS-Mal-Rhodamine, and PMBOxS-OND-Rhodamine were dissolved separately in PBS. The absorbance intensity of each solution was measured utilizing a UV-visible spectrophotometer, and they were diluted to ensure consistent absorbance intensity. These solutions were then injected into the tail base of C57BL/6 mice *via* subcutaneous injection. After 1, 2, 4, 7 and 15 days, the mice were euthanized, and inguinal LNs were harvested for fluorescence testing.

Tumor growth inhibition

3 × 10^5 B16-OVA cells were injected subcutaneously at the right flank of C57BL/6 mice on day 0 to establish the B16-OVA tumor model. The tumor-bearing mice were randomly divided into groups. On the 5th, 10th, and 15th days, the mice were administered with nanovaccine containing 20 μg of OVA peptide$_{257-264}$ *via* subcutaneous injection at the base of their tails. Tumor volume and mouse body weight were monitored on alternate days. The tumor volume was determined based on Vernier caliper measurements using the formula: tumor volume (V) = $a \times b^2/2$, where a denotes the long axis and b represents the short axis of the tumor.

ELISPOT assay

ELISPOT experiments were conducted to measure the antigen-specific response of T cells. Firstly, 100 μL of capture anti-IFN-γ antibody diluent was added to each well of an ELISPOT 96-well plate and incubated overnight at a temperature of 4 °C. Subsequently, the plate was blocked with 10% FBS in PBS for 2 hours. RPMI 1640 culture medium containing OVA peptide$_{257-264}$ was added to the wells. Fresh mouse splenocytes from the treatment group were then seeded into each well at a density of 3 × 10^5 cells per well and incubated at 37 °C for 72 hours. Afterward, the plate was incubated with anti-IFN-γ detection antibody diluent at room temperature for a period of 2 hours. This was followed by incubation with enzyme coupling (streptavidin-HRP) at room temperature for an hour, after which AEC solution was added to each well. The appearance of spots was monitored, and the reaction was terminated with deionized water.

Immune analysis after therapy

After the completion of treatment, blood samples were collected and mixed with heparin solution. The spleen was harvested and pulverized. Single-cell suspensions were then obtained by filtering through 300-mesh nylon strainers. Following this, red blood lysis buffer was introduced to the single-cell suspension, which was then re-suspended in FACS buffer to yield a single-cell suspension. Subsequently, the samples were stained using fluorochrome-conjugated antibodies, following the manufacturer's guidelines.

Statistical analysis

In all experiments, a minimum of three independent replicates were conducted, with the results presented as the mean ± standard deviation (s.d.). The statistical significance between two groups was determined using Student's *t*-test.

Results and discussion

Verification of the spontaneous release behavior of PMBOxSH conjugated cargos *via* the OND linker

POx emerges as an advantageous drug carrier owing to its inherent biocompatibility and versatile functionalization capabilities.[47–49] The polymer's ability to introduce a diverse array of functional groups enables precise manipulation and customization of drug carrier properties. To prepare amphiphilic polymer carriers containing free thiol groups, three 2-oxazoline monomers containing methyl, butyl, and thioether side groups were selected or synthesized. The hydrophobic 2-butyl-2-oxazoline was synthesized according to our previously reported method (Scheme S1, ESI†).[50] In brief, valeric acid was activated using ethyl chloroformate. Subsequently, this activated acid underwent a reaction with 2-chloroethylamine hydrochloride in the presence of TEA, resulting in the formation of intermediate molecules. Finally, 2-butyl-2-oxazoline was obtained by reacting with potassium carbonate. After purification, the monomer was obtained and the structure was verified *via* ^{1}H and ^{13}C NMR (Fig. S1 and S2, ESI†). Since the thiol group is not compatible with the living cationic ring opening polymerization of 2-oxazolines, we used 2-[2-(4-methoxybenzylsulfanyl)ethyl]-2-oxazoline (MOB-SOx) as the precursor

SH-functionalized monomer. To effectively obtain MOB-SOx, we resorted to Oskar Nuyken's approach[51] and optimized it as shown in Scheme S2 (ESI†). The first step includes the protection of 3-MPA, and the protected acid was then reacted with 2-chloroethylamine hydrochloride to yield the amide. Cyclization was achieved in the presence of K_2CO_3, resulting in the final product. The chemical structure of this final product was verified by ^{1}H NMR and ^{13}C NMR (Fig. S3–S6, ESI†).

The amphiphilic copolymer poly{(2-methyl-2-oxazoline)$_{80}$-*co*-[(2-butyl-2-oxazoline)$_{15}$-*r*-(MOB-SOx)$_8$]} (PMBSOx) was synthesized by cationic ring opening polymerization (CROP). The polymerization reactions were shown in Fig. 1a. 2-Methyl-2-oxazoline was firstly polymerized using MeOTf as the initiator. After 24 hours, 2-butyl-2-oxazoline and MOB-SOx monomers were added and reacted for another 48 hours to give the PMBSOx. The polymerization was terminated with methanolic NaOH (1 mol L^{-1}). ^{1}H NMR (Fig. 1b) confirmed the successful polymerization of all three monomers. The proportion of each monomer in the polymer was established by comparing the ratio of the characteristic signals of the three monomers (for MOB-SOx signal l, 2H at 6.8 ppm; for BuOx signal g, 3H at 0.9 ppm; for MeOx signal c, 3H at 2.15 ppm). Based on the integral values of characteristic peaks, the degrees of polymerization for MeOx, BuOx, and MOB-SOx were calculated to be 80, 15, and 8, respectively. The obtained PMBSOx was also evaluated using GPC (Fig. S7, ESI†). The number-average molecular weight (M_n) of PMBSOx was 10.1 kDa with a poly dispersion index (PDI) of 1.4.

Deprotection of the copolymers was performed in a mixture of trifluoroacetic acid and anisole, as shown in Scheme S3 (ESI†). Successful fragmentation is clearly indicated by the disappearance of the p-methoxybenzyl (PMB) ^{1}H NMR signal at δ = 6.8 ppm (signal l) and δ = 3.8 ppm (signal m) in Fig. 1b. The ability of thiol groups to quench FITC was used to show that free thiol groups were present in the PMBOxSH obtained. As shown in Fig. 1c, the existence of free sulfhydryl groups was demonstrated by the fact that FITC's fluorescence intensity dramatically reduced following the addition of PMBOxSH. Notably, the fluorescence intensity of FITC reduced more when 3-MPA was added, suggesting that some of the sulfhydryl groups in PMBOxSH may form disulfide bonds.

Previous studies reported that the thiol-OND adducts would undergo r-D–A fragmentation at room temperature spontaneously, resulting in furans and thiomalates, but the r-D–A cleavage of the original OND fragment would completely not appear in the absence of thiols.[44,52,53] That means OND may be an excellent linker for connecting carriers and the cargo for spontaneous cargo release. We synthesized the OND linker following M.G. Finn's method (Scheme S4, ESI†).[45] *N*-Glutaroylfurfurylamine was obtained by reacting furfurylamine with glutaric anhydride. In a single, very productive process, OND was easily obtained from cheap furans and dimethyl acetylenedicarboxylate. The chemical structure of the OND linker was verified by ^{1}H NMR (Fig. S8 and S9, ESI†).

OND is sulfhydryl-reactive and can undergo Michael addition reactions with sulfhydryl groups under alkaline conditions.[54]

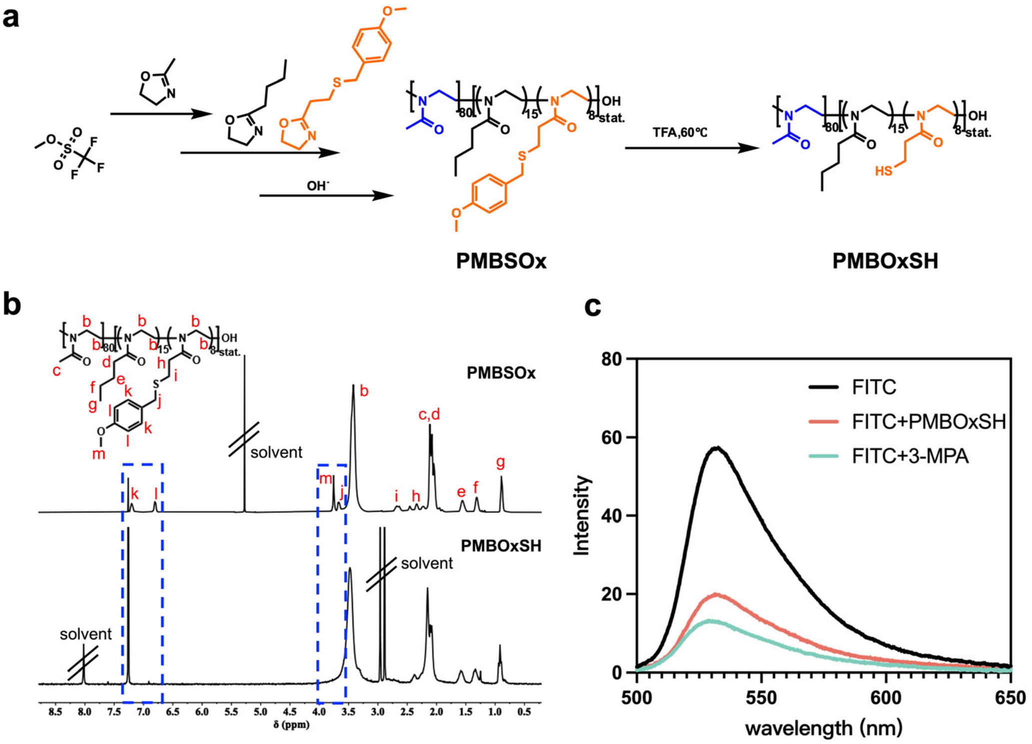

Fig. 1 Preparation and characterization of PMBOxSH. (a) Synthesis routes of PMBOxSH. (b) ^{1}H NMR spectra of PMBSOx and PMBOxSH in $CDCl_3$ (500 MHz). (c) Fluorescence curves of FITC mixed with PMBOxSH and 3-MPA, respectively.

The density of the electron cloud on the OND ring increases after the addition process, and the signal of the corresponding proton shifts to the right. We selected *n*-butyl mercaptan as the source of mercaptan to establish the reaction conditions (Scheme S5, ESI†). The *n*-butyl mercaptan and OND were dissolved in CD_3OD, then a catalytic quantity of TEA was added, and the mixture was monitored by ^1H NMR spectrum at 37 °C. The NMR signals for the a, b, and c protons on the OND ring of the feedstock persisted for 30 minutes of the process until they vanished after 60 minutes (Fig. S10, ESI†). This result demonstrated that the addition reaction of OND with sulfhydryl groups can be completed in less than 1 hour at 37 °C.

The stability of *n*-butyl mercaptan-OND adducts at different temperatures is critical for the preparation and storage of nanovaccine. The adduct is unstable and spontaneously undergoes a r-D–A reaction, releasing furans and olefins (Fig. 2a). The chemical shift of the a″ proton on the furan ring is around 7.4 ppm. Monitoring the r-D–A reaction can be achieved by observing the alteration in the integral value corresponding to δ = 7.4 ppm. To guarantee a sufficient reaction, we dissolved *n*-butyl mercaptan and OND in CD_3OD, added TEA, and allowed the mixture to stir at 37 °C for 1 hour. The reaction mixture was then separated into five portions and stored at 37 °C, 20 °C, 4 °C, −24 °C, and −80 °C to monitor the ^1H NMR spectrum changes (Fig. 2b and Fig. S11–S15, ESI†). At 37 °C, the OND-thiol adduct fragmented progressively over time at a decreasing pace, shattering 79% in 288 hours (Fig. 2c). At a temperature of 20 °C, the adducts' ability to fracture was greatly hindered; The adducts did not significantly fracture during the observation period when the temperature was decreased to 4 °C and below. This finding streamlines the subsequent production of nanovaccines, as it allows for the creation and storage of vaccine at lower temperatures. Moreover, when administered into the body, they may exhibit a gradual cargo release.

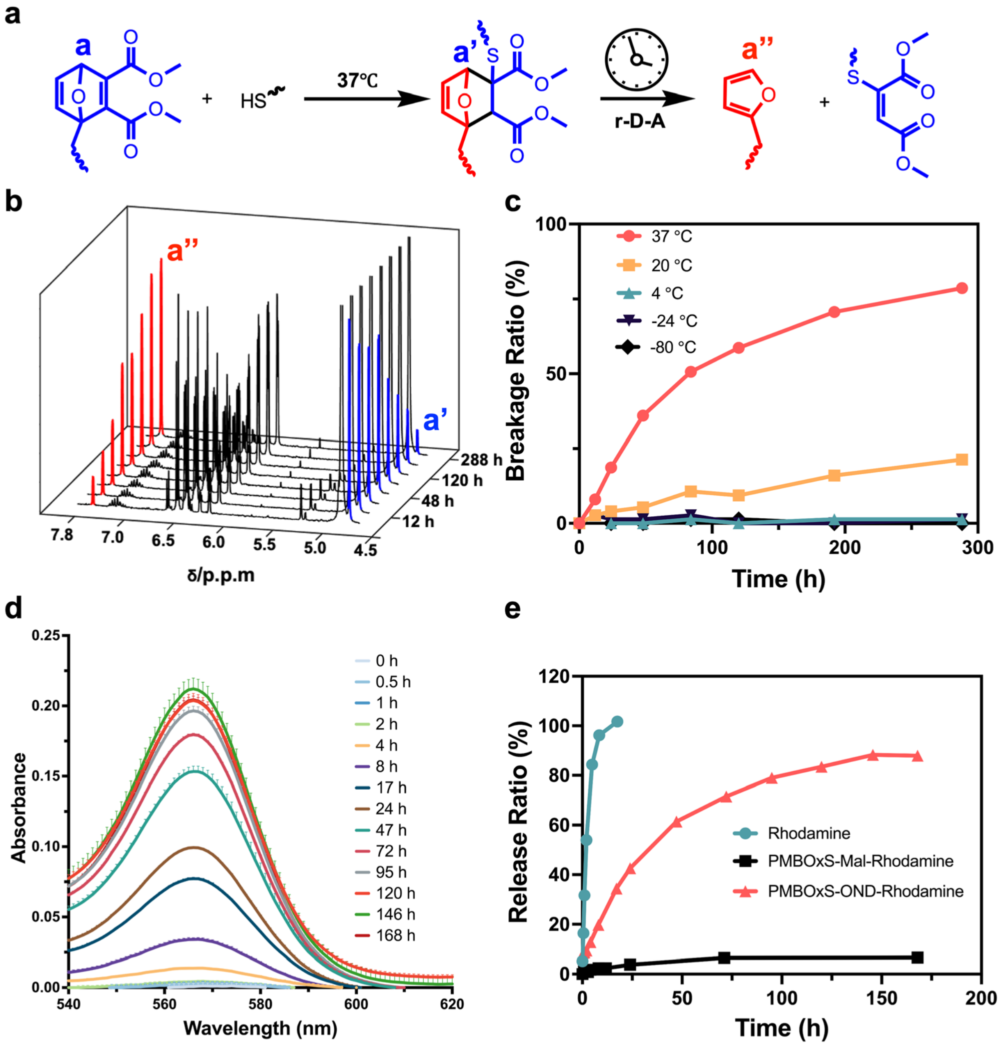

Fig. 2 (a) Reaction of ONDs with thios (*n*-butyl mercaptan) and fragmentation of adducts. (b) ^1H NMR spectrum for monitoring the r-D–A reaction at 37 °C (the spectra at the following time points are as follows: 0 h, 12 h, 24 h, 48 h, 84 h, 120 h, 192 h, and 288 h). (c) The curve depicting the rate of OND–thio adduct cleavage over time under different temperature conditions (37 °C, 20 °C, 4 °C, −24 °C and −80 °C). (d) UV-Visible absorption spectra of solutions released by PMBOxS-OND-Rhodamine under 37 °C conditions. (e) Release curves over time of RhoB piperazine amide, PMBOxS-Mal-Rhodamine, and PMBOxS-OND-Rhodamine in PBS under 37 °C conditions.

Continued stimulation of immune cells leads to a robust adaptive immune response.[55] To evaluate the release rate of nanovaccines *in vitro*, we employed RhoB as a marker molecule. However, an initial challenge arose as commercially available RhoB tends to undergo lactonization, resulting in diminished fluorescence.[56] Consequently, we initiated a modification process to address this limitation (Scheme S6 and Fig. S16, S17, ESI†).[57] Briefly, RhoB reacted with NaOH to yield RhoB base. The obtained RhoB base, when refluxed with piperazine and $AlMe_3$ in dichloromethane, yielded RhoB piperazine amide. To mimic the nanovaccine, PMBOxSH and OND reacted at 37 °C for 1 hour to yield PMBOxS-OND. Subsequently, utilizing EDC/NHS as a catalyst at 0 °C, the obtained PMBOxS-OND reacted with RhoB piperazine amide to produce PMBOxS-OND-Rhodamine (Scheme S7, ESI†). As a non-cleavable control, following the same method, OND was replaced with 3-maleimidopropionic acid to obtain PMBOxS-Mal-Rhodamine (Scheme S8, ESI†). To simulate the drug release process *in vitro*, we placed dialysis bags containing PMBOxS-OND-Rhodamine into beakers containing PBS, and then sealed the beakers for storage in a 37 °C shaking incubator. We examined the UV-visible absorption spectra of the solutions inside the beakers at various time intervals, as illustrated in Fig. 2d. With the passage of time, the UV-visible absorption intensity of the solutions inside the beakers gradually increased and eventually reached a stable level after 146 hours. We substituted PMBOxS-OND-Rhodamine with PMBOxS-Mal-Rhodamine or free RhoB piperazine amide, followed by testing the UV-visible absorption spectra of the solutions inside the beakers using the same method, and quantitatively summarized the results in Fig. 2e. The results showed that the free Rhodamine group exhibited complete release of Rhodamine molecules within 24 hours, whereas PMBOxS-Mal-Rhodamine demonstrated no significant release throughout the observation period. Notably, PMBOxS-OND-Rhodamine can achieve sustained release over a one-week period. These results indicate that nanovaccine linked *via* OND can achieve sustained and stable drug release under physiological conditions.

Preparation and characterization of the PMBOxS-OND-OVA/IMDQ nanovaccine

In the preparation of this nanovaccine, SIINFEKL, a variant of the chicken ovalbumin (OVA) MHC-I epitope, was chosen as a model antigen. Meanwhile, the Toll-like receptor 7/8 agonist IMDQ, selected for its potent immunostimulatory properties, was utilized as the adjuvant component in the nanovaccine formulation. The nanovaccine was prepared using a two-step method (Fig. 3a). Firstly, the reaction of PMBOxSH and OND was catalyzed by TEA at 37 °C for one hour, followed by cryodialysis to remove small molecule impurities.

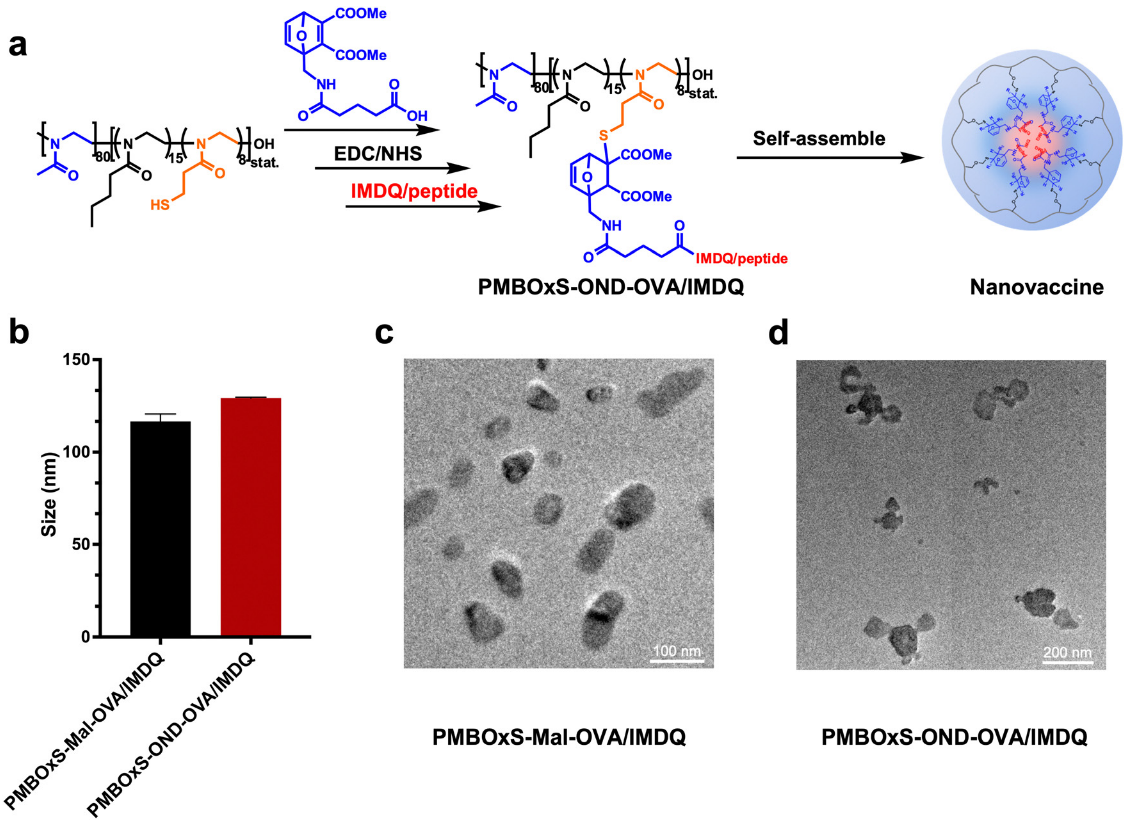

Fig. 3 (a) Schematic illustrations of the preparation of PMBOxS-OND-OVA/IMDQ nanovaccine. (b) Diameter of PMBOxS-Mal-OVA/IMDQ and PMBOxS-OND-OVA/IMDQ. (n = 3). (c) TEM image of PMBOxS-Mal-OVA/IMDQ. Scale bar = 100 nm. (d) TEM image of PMBOxS-OND-OVA/IMDQ. Scale bar = 200 nm.

Subsequently, in an ice-water bath, the dialysis products undergo a reaction with IMDQ/OVA under EDC/NHS catalysis. After 12 hours, the content of IMDQ and OVA in the mixed solution was detected *via* HPLC (Fig. S18, ESI†). The quantity of IMDQ and OVA bonded to the polymer was determined by subtracting the OVA/IMDQ content in the resulting mixed solution from the amount initially introduced. PMBOxS-OND showed good encapsulation ability for OVA and IMDQ, with drug loading content (DLC %) of 13.0 wt% and 2.4 wt%, respectively. Finally, the PMBOxS-OND-OVA/IMDQ nanovaccine was obtained through low-temperature ultrafiltration.

Maleimide is capable of reacting with sulfhydryl groups and the reaction products are relatively stable. As a control, we utilized 3-maleimidopropionic acid to bond OVA/IMDQ to PMBOxSH. The OND was replaced with 3-maleimidopropionic acid, and the same preparation method as PMBOxS-OND-OVA/IMDQ was used to obtain PMBOxS-Mal-OVA/IMDQ nanovaccine (Scheme S9, ESI†). The DLC % of PMBOxS-Mal for OVA and IMDQ was 14.3 wt% and 3.2 wt%, respectively (Fig. S19, ESI†). To confirm the successful assembly of the nanovaccine, the hydrodynamic sizes of the PMBOxS-Mal-OVA/IMDQ nanovaccine and PMBOxS-OND-OVA/IMDQ nanovaccine were measured *via* DLS to be 117 ± 3 nm and 129 ± 3 nm, respectively (Fig. 3b). TEM results further validated the successful assembly of the nanovaccines (Fig. 3c and d).

Activation and antigen presentation of PMBOxS-OND-OVA/IMDQ nanovaccine in DCs *in vitro* and *in vivo*

A large number of DCs are present in the LNs,[58] and these cells phagocytize, process antigens and present them to $CD8^+$ T cells *via* MHC-I molecules, which further induces antigen-specific cytotoxic T-cell responses.[59,60] The up-regulated expression of costimulatory molecules is a typical sign of the maturation of DCs (Fig. 4a). After incubation of BMDCs with nanovaccines *in vitro*, the expression of CD86 and MHC II was investigated *via* flow cytometry. As depicted in Fig. 4b, a significant up-regulation of CD86 expression was observed in BMDCs co-incubated with PMBOxS-Mal-OVA/IMDQ and PMBOxS-OND-OVA/IMDQ, compared to the PBS group. This suggests that IMDQ bonded to polymers still has the ability to promote DC maturation. In addition, PMBOxS-Mal-OVA/IMDQ and PMBOxS-OND-OVA/IMDQ induced the significantly up-regulated expression of MHC II on BMDCs, suggesting the enhanced capability to prime $CD4^+$ T cells through the MHC II pathway (Fig. S20, ESI†). Next, we investigated the antigen presentation efficiency for DCs incubated with nanovaccines. The result revealed that PMBOxS-OND-OVA/IMDQ exhibited the significantly up-regulated expression of SIINFEKL-MHC I on BMDCs (Fig. 4c and Fig. S21, ESI†), which was essential for the activation of cytotoxic $CD8^+$ T cells. Notably, BMDCs incubated with PMBOxS-Mal-OVA/IMDQ presented a similar level of SIINFEKL-H2Kb to the control PBS group, suggesting OVA peptide conjugated *via* the Mal linker could not be efficiently released and presented in DCs.

Encouraged by the findings observed *in vitro*, we subsequently evaluated the immune responses elicited by the nanovaccines *in vivo*. C57BL/6 mice were subcutaneously injected at the base of the tail with free OVA/IMDQ, PMBOxS-Mal-OVA/IMDQ nanovaccine or PMBOxS-OND-OVA/IMDQ nanovaccine with equivalent OVA $peptide_{257-264}$ amount. Inguinal LNs were collected 48 hours post-immunization to assess the immunization efficacy. As shown in Fig. 4d, compared to the free OVA/IMDQ group, nanovaccines treatment significantly promoted the maturation of DCs within the inguinal LNs. Consistent with the *in vitro* findings, PMBOxS-OND-OVA/IMDQ nanovaccine significantly enhanced the expression of CD80 and CD86 on DCs within the LNs, attributable to the intrinsic immunoadjuvant effect of IMDQ (Fig. S22, ESI†). Similarly, we also observed a significant increase in the percentage of $CD11c^+$SIINFEKL-$H2Kb^+$ DCs in the PMBOxS-OND-OVA/IMDQ nanovaccine treatment group (Fig. 4e and Fig. S23, ESI†). However, it is noteworthy that there was no significant difference in the percentage of $CD11c^+$SIINFEKL-$H2Kb^+$ DCs between the PMBOxS-Mal-OVA/IMDQ nanovaccine treatment group and the free OVA/peptide treatment group. This may be attributed to the ineffective peptide release by the nanovaccine conjugated *via* the Mal linker.

Lymph node draining of the PMBOxS-OND-OVA/IMDQ nanovaccine

LNs are the primary site for inducing cellular and humoral immunity, where antigens are taken up, processed and presented by APCs thereby activating naïve T cells. There is an urgent need for vaccines that can deliver antigens and adjuvants efficiently to the LNs. To assess the ability of nanovaccines to reach and accumulate in LNs, PMBOxS-OND-Rhodamine, PMBOxS-Mal-Rhodamine and RhoB were injected subcutaneously into the tail base of C57BL/6 mice at a volume of 100 μL. Following 24 and 48 hours post-injection, the inguinal LNs on both sides were excised and photographed using an *in vivo* imaging system (Fig. 5a). As shown in Fig. 5b, the free Rhodamine group showed a very weak fluorescent signal in the LNs. After conjugating to PMBOxS-Mal and PMBOxS-OND, the fluorescence intensity in LNs increased 3.1 and 4.0-fold than free Rhodamine at 48 hours (Fig. 5c), certifying that the PMBOxSH carrier could increase the LN reflux capacity. Next, to investigate the release kinetics of the nanovaccines *in vivo*, LNs were harvested and imaged in a range of time after immunization with free Rhodamine, PMBOxS-Mal-Rhodamine and PMBOxS-OND-Rhodamine (Fig. S24, ESI†). 2 days after inoculation, the fluorescence intensity of the free Rhodamine group in the LN reduced to the basal level (Fig. 5d). Although fluorescence signal was observed in all nanovaccine groups over the initial 7 days, the fluorescence intensity in the LN of the PMBOxS-Mal-Rhodamine group showed less decline in 15 days, while the fluorescence intensity of PMBOxS-OND-Rhodamine in the LN continued to decline and decreased to the basal level in 15 days. These results demonstrate that PMBOxSH carrier can achieve LN residency for up to 15 days, while OND-bonded nanovaccine can achieve sustained release in the LNs.

We conducted an in-depth analysis of the intra-LN distribution of fluorescent signals utilizing CLSM. As depicted in

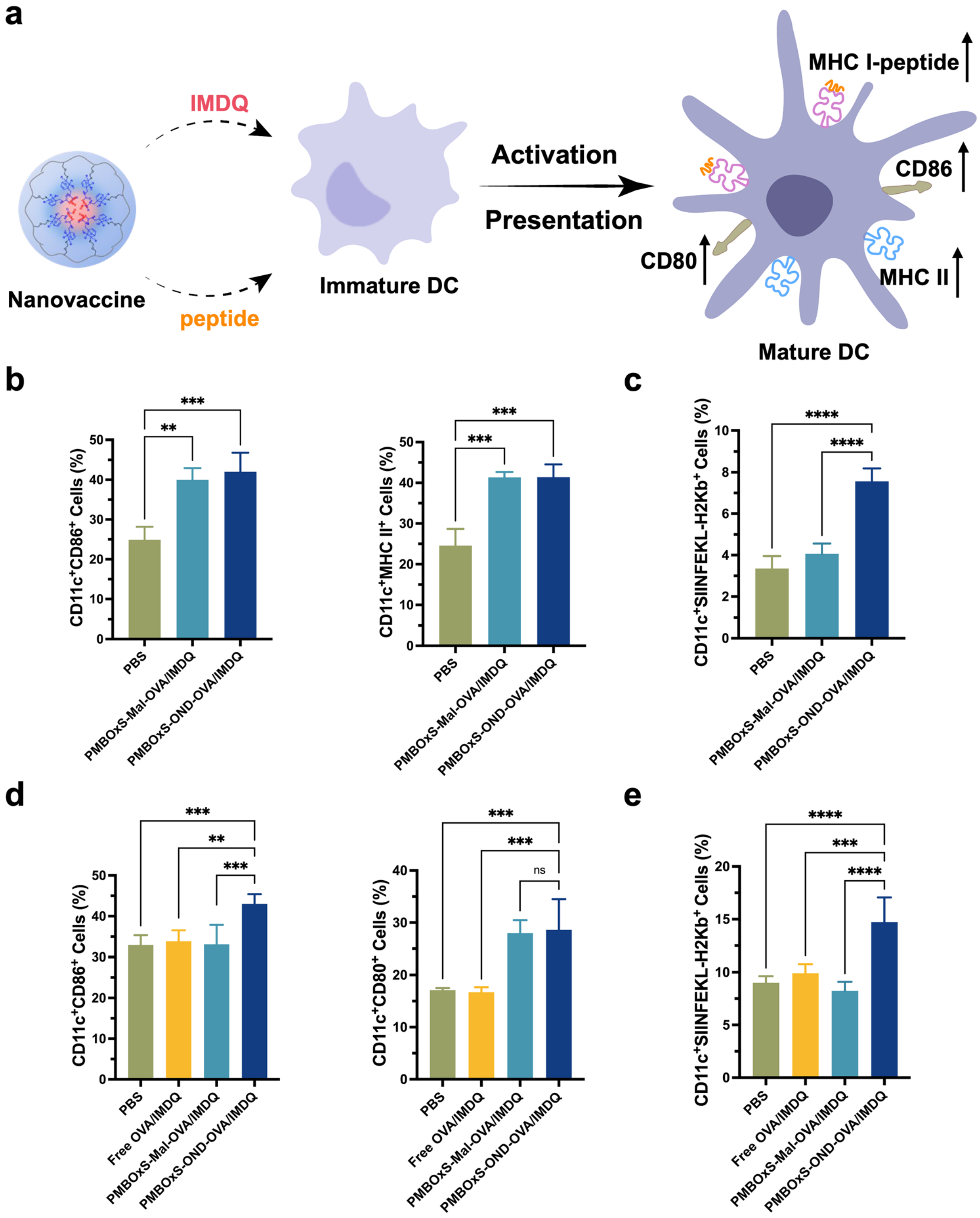

Fig. 4 (a) The nanovaccine induces activation and cross-presentation of DCs. (b) BMDC activation effect in different vaccine treatment groups (*n* = 3). (c) Antigen cross-presentation results of BMDCs in various treatment groups (*n* = 5). (d) and (e) FACS analysis of DC surface markers (CD80, CD86) and antigen cross-presentation (SIINFEKL-H2Kb) in inguinal draining LNs after subcutaneous injection of different vaccine formulations (*n* = 5). Results are presented as mean ± sd; **p* < 0.05, ***p* < 0.01, ****p* < 0.001, *****p* < 0.0001; ns, no significance.

Fig. 5e, no significant presence of Rhodamine signals was detected within the LN in the free Rhodamine group at the time of observation. However, a majority of Rhodamine signals were predominantly observed on the edge of the LN in the PMBOxS-Mal-Rhodamine group. In contrast, more extensive and deeper penetration of Rhodamine was noted in the PMBOxS-OND-Rhodamine group at 4 and 7 days (Fig. S25, ESI†). Collectively, these findings underscore that OND-bonded nanovaccine can achieve enrichment in LNs and their released cargos possess the capability to penetrate deeply into LNs.

Tumor therapy results of PMBOxS-OND-OVA/IMDQ nanovaccine on the B16-OVA tumor model

Motivated by the excellent ability of PMBOxS-OND-OVA/IMDQ in LN reflux, LN infiltration, DC activation and antigen presentation, we further investigated the anti-tumor effects of the nanovaccine. 3 × 10^5 B16-OVA cells were injected

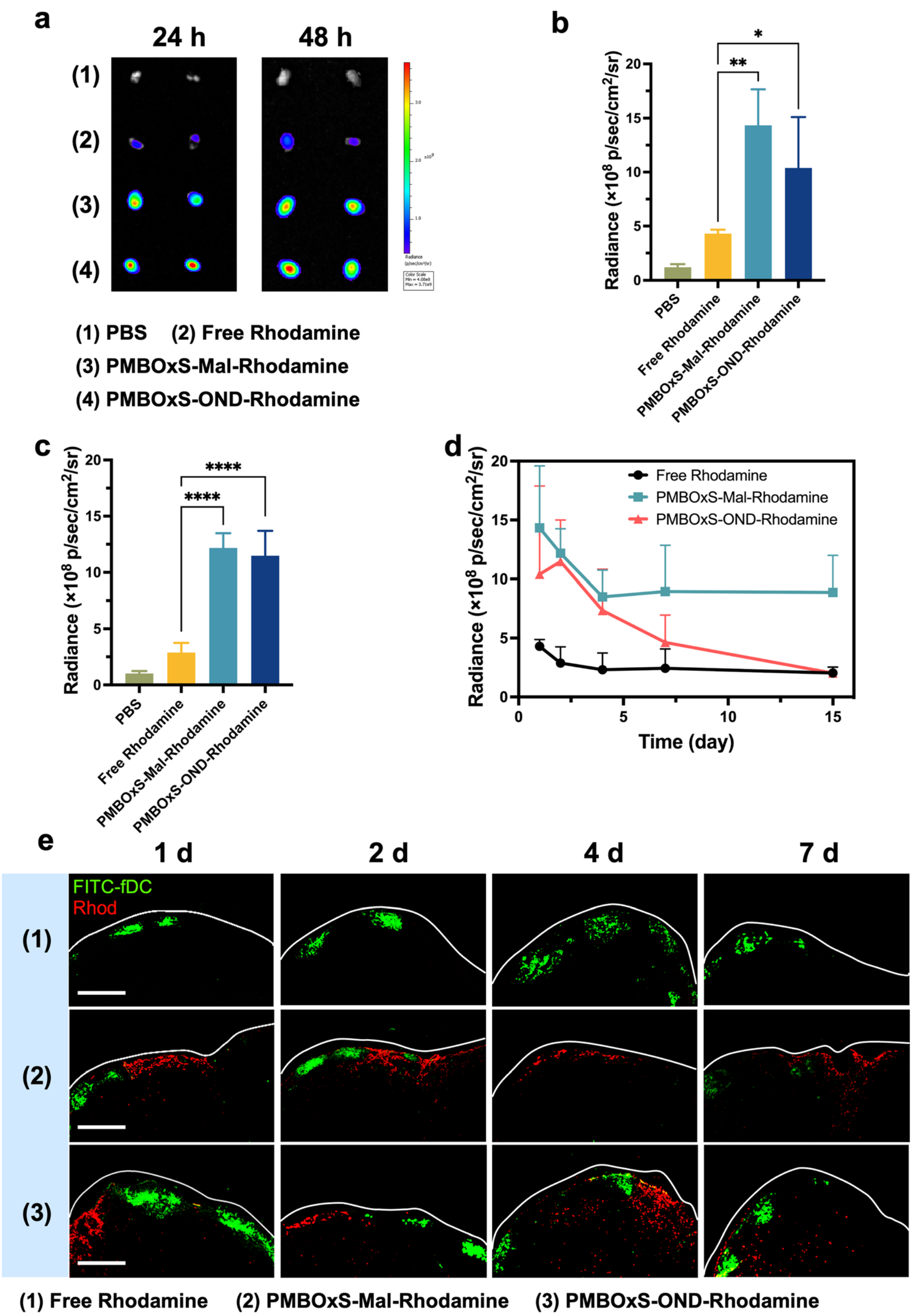

Fig. 5 (a) *Ex vivo* fluorescent images of LNs in different treatment groups. Mice were subcutaneously injected with 100 μL of different formulations and LNs were excised after 1 d and 2 d. (b) and (c) The fluorescence intensity of Rhodamine from different vaccines in LNs of mice 24 h (b) and 48 h (c) after immunization. (d) The fluorescence intensity of distribution of different vaccines in LNs at 1, 2, 4, 7, and 15 d after immunization with different treatment groups. (e) CLSM images of Rhodamine distribution in LNs of different treatment groups. Drawn white lines indicate the outer contour of LNs (scale bar = 200 μm).

subcutaneously at the right flank of C57BL/6 mice on day 0 to establish the B16-OVA tumor model. The mice were randomly divided into the following four groups: (1) PBS, (2) Free OVA/IMDQ, (3) PMBOxS-Mal-OVA/IMDQ, and (4) PMBOxS-OND-OVA/IMDQ. Treatments were given to each group on days 5, 10, and 15. Tumor volume and body weights were measured on alternate days. The mice were given 100 μL volume subcutaneous injections at the base of the tail, with 20 μg of OVA peptide$_{257-264}$ administered for each injection (Fig. 6a). As shown in Fig. 6b, in contrast to PBS, free OVA/IMDQ, and PMBOxS-Mal-OVA/IMDQ, PMBOxS-OND-OVA/IMDQ dramatically slowed tumor growth, demonstrating the significance of

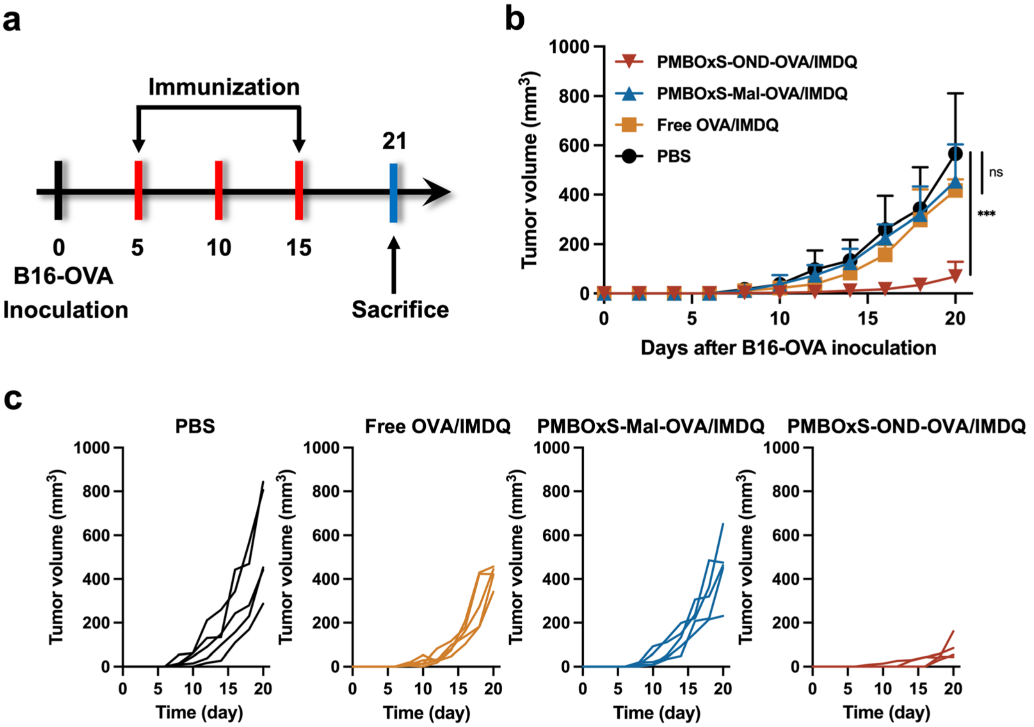

Fig. 6 (a) Schematic illustration of tumor inoculation and treatment schedule. (b) and (c) Average (b) and individual (c) tumor growth curves of mice in different treatment groups (n = 5). (ns: not significant, *$p < 0.05$, **$p < 0.01$, ***$p < 0.001$).

antigen and adjuvant deep LN penetration for anticancer efficacy. On day 20, the PMBOxS-OND-OVA/IMDQ group had a tumor suppression rate (TSR%) of 88%, while no other treatment groups had a statistically meaningful antitumor

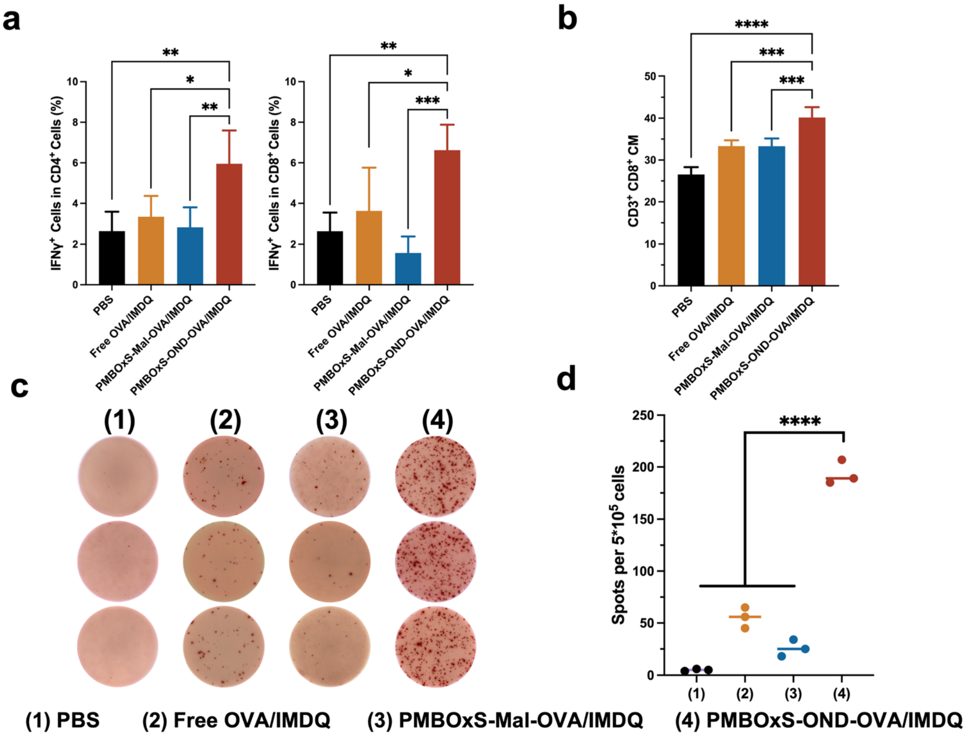

Fig. 7 (a) FACS analysis of IFN-γ positive T cells in the peripheral blood on the 5th day after three vaccinations. (b) Memory T cells in the spleens after various treatments on day 21. (c) ELISPOT results of splenocytes from different treatment groups. (d) Spot counts of ELISPOT analysis from different treatment groups. (n = 3). (ns: not significant, *$p < 0.05$, **$p < 0.01$, ***$p < 0.001$, ****$p < 0.0001$).

effect (Fig. 6c and Fig. S26, ESI†). No significant reductions in body weight were noted across all groups (Fig. S27, ESI†), suggesting the safety of these interventions, which is further supported by the absence of cytotoxicity *in vitro* (Fig. S28, ESI†).

Mice were executed on day 21 and then immune cells in blood and spleen were analyzed. To validate the immune activation induced by nanovaccines, T cells were detected by flow cytometry. As depicted in Fig. 7a, a significant elevation was observed in both IFN-γ^+ CD4$^+$ and IFN-γ^+ CD8$^+$ T cell populations in the blood following PMBOxS-OND-OVA/IMDQ treatment. However, no substantial alterations were noted in the remaining groups (Fig. S29, ESI†). The blood immune cell analysis supported the anticancer results. A potent immune memory effect can activate the immune response when encountering the same antigen again, thus preventing tumor recurrence. Subsequent examination of memory cell subsets in the mouse spleen following various treatments revealed a significant increase in CD8$^+$ central memory (CM) T cells post PMBOxS-OND-OVA/IMDQ treatment (Fig. 7b and Fig. S30, ESI†). Compared with PMBOxS-Mal-OVA/IMDQ, PMBOxS-OND-OVA/IMDQ induced the production of more CD8$^+$ CM, which suggested that OND-bonded nanovaccine can evoke robust immune memory responses. ELISPOT analysis was carried out to further demonstrate that PMBOxS-OND-OVA/IMDQ may trigger antigen-specific T-cell responses. The isolated splenocytes were co-incubated with the OVA peptide$_{257-264}$ for a duration of 72 hours. Notable spots were evident in the PMBOxS-OND-OVA/IMDQ treated group, which further demonstrated the potent *in vivo* antigen-specific T-cell immune responses elicited by the PMBOxS-OND-OVA/IMDQ nanovaccine (Fig. 7c and d). All these results demonstrated that the PMBOxS-OND-OVA/IMDQ nanovaccine could effectively inhibit tumor growth and trigger robust antigen-specific T-cell responses.

Conclusions

In this study, we developed a dynamic release nanovaccine based on the r-D–A reaction for triggering a robust anti-tumor cellular immune response. As a delivery vehicle, PMBOxSH was able to reflux well to the LNs and reside there for a long time (>15 days). According to the findings, the PMBOxS-OND-OVA/IMDQ nanovaccine could maintain the release of cargo in the LNs and allow that cargo to reach a significant depth inside the LNs. In addition, *in vitro* and *in vivo* experiments demonstrated that our designed nanovaccine can activate DCs and promote DCs to present antigenic peptides. In the B16-OVA tumor model, the administration of the PMBOxS-OND-OVA/IMDQ nanovaccine resulted in superior antitumor effects, with an 88% tumor suppression rate (TSR%). These results demonstrate that effective transport of antigen and adjuvant to the deeper layers of LNs is critical for inducing potent adaptive immunity.

Author contributions

Kuncheng Lv: conceptualization, methodology, and original draft preparation. Sheng Ma: methodology. Liping Liu, Hongyu Chen and Zichao Huang: visualization and investigation. Zhenyi Zhu and Yibo Qi: formal analysis and investigation. Wantong Song: project administration, writing, funding acquisition, and validation.

Conflicts of interest

The authors declare that they have no conflicts of interest in this work.

Acknowledgements

This work was supported by grants from the National Natural Science Foundation of China (22222509, 22375198, 52103194, and 22105199), the Bureau of International Cooperation Chinese Academy of Sciences (121522KYSB20200029), the Jilin Provincial International Cooperation Key Laboratory of Biomedical Polymers (20210504001GH), the Jilin Province Development and Reform Commission (2023C043-4), and the Jilin Province Science and Technology Development Plan (20220402037GH).

Notes and references

1 M. J. Lin, J. Svensson-Arvelund, G. S. Lubitz, A. Marabelle, I. Melero, B. D. Brown and J. D. Brody, *Nat. Cancer*, 2022, **3**, 911–926.

2 C. L. Slingluff, Jr., *Cancer J.*, 2011, **17**, 343–350.

3 L. Zhang, Y. Huang, A. R. Lindstrom, T. Y. Lin, K. S. Lam and Y. Li, *Theranostics*, 2019, **9**, 7807–7825.

4 M. A. Cheever and C. S. Higano, *Clin. Cancer Res.*, 2011, **17**, 3520–3526.

5 X. Hu, N. G. Chakraborty, J. R. Sporn, S. H. Kurtzman, M. T. Ergin and B. Mukherji, *Cancer Res.*, 1996, **56**, 2479–2483.

6 Y. Yoshitake, D. Fukuma, A. Yuno, M. Hirayama, H. Nakayama, T. Tanaka, M. Nagata, Y. Takamune, K. Kawahara, Y. Nakagawa, R. Yoshida, A. Hirosue, H. Ogi, A. Hiraki, H. Jono, A. Hamada, K. Yoshida, Y. Nishimura, Y. Nakamura and M. Shinohara, *Clin. Cancer Res.*, 2015, **21**, 312–321.

7 W. Song, S. N. Musetti and L. Huang, *Biomaterials*, 2017, **148**, 16–30.

8 G. Zhu, F. Zhang, Q. Ni, G. Niu and X. Chen, *ACS Nano*, 2017, **11**, 2387–2392.

9 S. T. Reddy, A. J. van der Vlies, E. Simeoni, V. Angeli, G. J. Randolph, C. P. O'Neil, L. K. Lee, M. A. Swartz and J. A. Hubbell, *Nat. Biotechnol.*, 2007, **25**, 1159–1164.

10 S. N. Thomas and A. Schudel, *Curr. Opin. Chem. Eng.*, 2015, **7**, 65–74.

11 H. Chen, Z. Huang, J. Li, S. Dong, Y. Xu, S. Ma, J. Zhao, L. Liu, T. Sun, W. Song and X. Chen, *Sci. Bull.*, 2024, **69**, 922–932.

12 L. Liu, J. Zhao, Z. Huang, Y. Xu, H. Chen, R. Qiao, W. Song, Z. Tang, T. P. Davis and X. Chen, *Fundam. Res.*, 2023, DOI: **10.1016/j.fmre.2023.03.018**.

13 M. Y. Gerner, P. Torabi-Parizi and R. N. Germain, *Immunity*, 2015, **42**, 172–185.

14 Y. Xu, S. Ma, J. Zhao, H. Chen, X. Si, Z. Huang, Z. Yu, W. Song, Z. Tang and X. Chen, *Biomaterials*, 2022, **284**, 121489.

15 M. F. Bachmann and G. T. Jennings, *Nat. Rev. Immunol.*, 2010, **10**, 787–796.

16 X. Si, W. Song and X. Chen, *Acta Polym. Sin.*, 2023, **54**, 837–852.

17 O. P. Joffre, E. Segura, A. Savina and S. Amigorena, *Nat. Rev. Immunol.*, 2012, **12**, 557–569.

18 D. S. Chen and I. Mellman, *Immunity*, 2013, **39**, 1–10.

19 C. Wong, T. Stylianopoulos, J. Cui, J. Martin, V. P. Chauhan, W. Jiang, Z. Popović, R. K. Jain, M. G. Bawendi and D. Fukumura, *Proc. Natl. Acad. Sci. U. S. A.*, 2011, **108**, 2426–2431.

20 Y. Zhang, S. Ma, X. Liu, Y. Xu, J. Zhao, X. Si, H. Li, Z. Huang, Z. Wang, Z. Tang, W. Song and X. Chen, *Adv. Mater.*, 2021, **33**, 2007293.

21 S. Ma, W. Song, Y. Xu, X. Si, Y. Zhang, Z. Tang and X. Chen, *CCS Chem.*, 2020, **2**, 390–400.

22 R. de la Rica, D. Aili and M. M. Stevens, *Adv. Drug Delivery Rev.*, 2012, **64**, 967–978.

23 V. Estrella, T. Chen, M. Lloyd, J. Wojtkowiak, H. H. Cornnell, A. Ibrahim-Hashim, K. Bailey, Y. Balagurunathan, J. M. Rothberg, B. F. Sloane, J. Johnson, R. A. Gatenby and R. J. Gillies, *Cancer Res.*, 2013, **73**, 1524–1535.

24 K. Wang, G. Luo, Y. Liu, C. Li, S. Cheng, R. Zhuo and X. Zhang, *Polym. Chem.*, 2012, **3**, 1084–1090.

25 K. M. Holmström and T. Finkel, *Nat. Rev. Mol. Cell Biol.*, 2014, **15**, 411–421.

26 S. Mishra, S. S. Verma, V. Rai, N. Awasthee, J. S. Arya, K. K. Maiti and S. C. Gupta, *Biomolecules*, 2019, **9**, 159.

27 J. Chen, J. Ding, Y. Wang, J. Cheng, S. Ji, X. Zhuang and X. Chen, *Adv. Mater.*, 2017, **29**, 1701170.

28 X. Guo, X. Wei, Y. Jing and S. Zhou, *Adv. Mater.*, 2015, **27**, 6450–6456.

29 T. Cui, Z. Yan, H. Qin, Y. Sun, J. Ren and X. Qu, *Small*, 2019, **15**, 1903323.

30 Y. Lee, T. Ishii, H. J. Kim, N. Nishiyama, Y. Hayakawa, K. Itaka and K. Kataoka, *Angew. Chem., Int. Ed.*, 2010, **49**, 2552–2555.

31 S. Chen, J. Zheng, L. Li and S. Jiang, *J. Am. Chem. Soc.*, 2005, **127**, 14473–14478.

32 J. Du, H. Li and J. Wang, *Acc. Chem. Res.*, 2018, **51**, 2848–2856.

33 D. Koda, T. Maruyama, N. Minakuchi, K. Nakashima and M. Goto, *Chem. Commun.*, 2010, **46**, 979–981.

34 D. Cheng, X. Zhang, Y. Gao, L. Ji, D. Hou, Z. Wang, W. Xu, Z. Qiao and H. Wang, *J. Am. Chem. Soc.*, 2019, **141**, 7235–7239.

35 Z. Wang, Y. Wang, X. Jia, Q. Han, Y. Qian, Q. Li, J. Xiang, Q. Wang, Z. Hu and W. Wang, *Theranostics*, 2019, **9**, 1728–1740.

36 Y. Gao, H. Zhao, J. Zhao, S. Ma, X. Si, L. Liu, R. Qiao, W. Song and X. Chen, *Sci. China: Chem.*, 2023, **66**, 3576–3586.

37 H. Jiang, Q. Wang and X. Sun, *J. Controlled Release*, 2017, **267**, 47–56.

38 S. J. Rowan, S. J. Cantrill, G. R. L. Cousins, J. K. M. Sanders and J. F. Stoddart, *Angew. Chem., Int. Ed.*, 2002, **41**, 898–952.

39 S. Huang, X. Kong, Y. Xiong, X. Zhang, H. Chen, W. Jiang, Y. Niu, W. Xu and C. Ren, *Eur. Polym. J.*, 2020, **141**, 110094.

40 P. Taynton, K. Yu, R. K. Shoemaker, Y. Jin, H. J. Qi and W. Zhang, *Adv. Mater.*, 2014, **26**, 3938–3942.

41 G. Deng, F. Li, H. Yu, F. Liu, C. Liu, W. Sun, H. Jiang and Y. Chen, *ACS Macro Lett.*, 2012, **1**, 275–279.

42 J. Zhao, R. Xu, G. Luo, J. Wu and H. Xia, *J. Mater. Chem. B*, 2016, **4**, 982–989.

43 L. Feng, Z. Yu, Y. Bian, J. Lu, X. Shi and C. Chai, *Polymer*, 2017, **124**, 48–59.

44 M. Mahajna, G. B. Quistad and J. E. Casida, *Chem. Res. Toxicol.*, 1996, **9**, 241–246.

45 C. J. Higginson, S. Y. Kim, M. Peláez-Fernández, A. Fernández-Nieves and M. G. Finn, *J. Am. Chem. Soc.*, 2015, **137**, 4984–4987.

46 A. Schudel, A. P. Chapman, M.-K. Yau, C. J. Higginson, D. M. Francis, M. P. Manspeaker, A. R. C. Avecilla, N. A. Rohner, M. G. Finn and S. N. Thomas, *Nat. Nanotechnol.*, 2020, **15**, 491–499.

47 N. Adams and U. S. Schubert, *Adv. Drug Delivery Rev.*, 2007, **59**, 1504–1520.

48 R. Hoogenboom, *Angew. Chem., Int. Ed.*, 2009, **48**, 7978–7994.

49 R. Hoogenboom, *Eur. Polym. J.*, 2022, **179**, 111521.

50 S. Dong, S. Ma, Z. Liu, L. Ma, Y. Zhang, Z. Tang, M. Deng and W. Song, *Chin. J. Polym. Sci.*, 2021, **39**, 865–873.

51 S. Cesana, A. Kurek, M. A. Baur, J. Auernheimer and O. Nuyken, *Macromol. Rapid Commun.*, 2007, **28**, 608–615.

52 V. Hong, A. A. Kislukhin and M. G. Finn, *J. Am. Chem. Soc.*, 2009, **131**, 9986–9994.

53 A. A. Kislukhin, C. J. Higginson, V. P. Hong and M. G. Finn, *J. Am. Chem. Soc.*, 2012, **134**, 6491–6497.

54 S. Albert, A. Soret, L. Blanco and S. Deloisy, *Tetrahedron*, 2007, **63**, 2888–2900.

55 B. S. Ou, O. M. Saouaf, J. Baillet and E. A. Appel, *Adv. Drug Delivery Rev.*, 2022, 187.

56 M. Adamczyk and J. Grote, *Bioorg. Med. Chem. Lett.*, 2003, **13**, 2327–2330.

57 T. Nguyen and M. B. Francis, *Org. Lett.*, 2003, **5**, 3245–3248.

58 A. A. Itano, S. J. McSorley, R. L. Reinhardt, B. D. Ehst, E. Ingulli, A. Y. Rudensky and M. K. Jenkins, *Immunity*, 2003, **19**, 47–57.

59 H. Ueno, E. Klechevsky, R. Morita, C. Aspord, T. Cao, T. Matsui, T. Di Pucchio, J. Connolly, J. W. Fay, V. Pascual, A. K. Palucka and J. Banchereau, *Immunol. Rev.*, 2007, **219**, 118–142.

60 Z. Zhu, W. Song and X. Chen, *Acta Polym. Sin.*, 2023, **54**, 534–549.